Proceedings of the 23rd National Heat and Mass Transfer Conference and
1st International ISHMT-ASTFE Heat and Mass Transfer Conference
IHMTC2015
17-20 December, 2015, Thiruvananthapuram, India

IHMTC2015- 602

EFFECT OF NOZZLE DIVERGENCE ANGLE ON PLUME EXPANSION IN OUTER-SPACE CONDITIONS

A Bhagat
Department of Mechanical &
Aerospace Engineering/IIT Hyderabad
Student
Email: me13m15p000001@iith.ac.in

D R Mopuru
Department of Mechanical &
Aerospace Engineering/IIT Hyderabad
Student
Email: me14resch11012@iith.ac.in

Dr N Dongari
Department of Mechanical &
Aerospace Engineering/IIT Hyderabad
Assistant professor
Email: nishanth@iith.ac.in

Dr V K Saraswat
DAE Homi Bhabha Chair &
Aerospace Engineering/IIT Hyderabad
Email: vksaraswat1949@gmail.com

ABSTRACT

We carry out numerical simulations to investigate the effect of nozzle divergence angle on back flow of plume expansion into rarefied atmosphere. Results are obtained using open source compressible computational fluid dynamics (CFD) solver. Non-equilibrium slip and jump boundary conditions for velocity and temperature are implemented to capture rarefaction rarefaction effects in the slip flow regime. The solver has been validated with the experimental data for a nozzle flow in the slip flow regime. We explore the non-linear non-equilibrium gas flow physics of a supersonic jet expansion. We report results of pressure, heat and drag coefficients for different divergent angles (12^0, 15^0 and 20^0) at 80 km altitude conditions. The slip based results for heat loads significantly under-predict the no-slip ones, while for pressure and drag coefficients, deviations are found to be minute. It is noticed that thrust coefficient of nozzle increases with increase in divergence angle, however, nozzle with divergent angle of 15^0 led to minimum drag and heat transfer load on the critical region. The current study is important from the perspective of the overall aero-thermodynamic design of a typical supersonic rocket model operating under rarefied conditions.

***Keywords*:** divergence angle, backflow, plume expansion

NOMENCLATURE

C_h pressure coefficient
C_D drag coefficient
p pressure
T temperature
U velocity
U_x axial velocity
U_y radial velocity
c_p specific heat at constant pressure
k thermal conductivity
R gas constant
B Reynolds number
Pr Prandtl number
Kn Knudsen number
Ma Mach number
ρ density

λ mean free path
μ dynamic viscosity
σ_v tangential momentum accommodation coefficient
σ_T thermal accommodation coefficient
γ ratio of specific heats
∞ free-stream condition
0 stagnation condition
τ_w wall shear stress

1 INTRODUCTION

Supersonic under-expanded jet plumes in the rarefied atmosphere lead to back flow phenomenon [1]. The characteristics of the back flow phenomenon depend significantly on the rarefied conditions and it is also found to be sensitive to the nozzle divergence angle. The back flow effect causes unanticipated aero-thermodynamics effects like enhancement of heat load, excessive contamination from plume gases and erosion of critical surfaces [2]. Special shielding will be required on critical parts, if the back flow is detrimental to the planned operation of Aerospace systems. Therefore, an accurate prediction of aero-thermodynamic loads due to plume backflow and interaction with supersonic freestreams on critical parts is necessary for aerospace applications.

Early investigations on under-expanded exhaust plumes consist of experiments supplemented by method of characteristics and shock expansion techniques [3–6].

Biju *et al* [7] and Patel [8] performed CFD analysis to understand supersonic over-expanded nozzle at different divergence angles. They obtained the optimum divergent angle where shock instabilities were eliminated. Campbell *et al* [9] obtained nozzle performance data at high pressure ratio for different half divergent angles and area ratios. Krull *et al* [10] explained the effect of thrust coefficient on various factors like exit pressure ratio, nozzle divergent angle. Steffen *et al* [11] conducted experiments on over-expanded nozzles for wide range of divergent angles, to study the effect of separation at different pressure ratios.

The existing commercial CFD tools are only valid in the continuum regime, i.e. altitude less than 40 km. While DSMC simulations are computationally intensive as the practical problems involve the continuum plume jet at the exit of the nozzle and not so feasible for 2-D/3-D large scale nozzle geometries. Alternatively, few researchers have been rigorously exploring extended hydrodynamic methods, such as applying non-equilibrium boundary conditions at the wall surfaces [12–14] and/or employing non-linear/higher-order constitutive relations [15–17]. These attempts have been carried out within the Naviers-Stokes equations framework to extend their applicability upto the slip flow regime, i.e. to cover altitudes from 60 to 90 km. On the other hand, the effect of nozzle divergence angle on back flow phenomenon and various performance parameters was done at lower altitudes only i.e., less than 30 km.

In the current paper, we investigate the effect of nozzle divergence angle on under-expanded plumes in the rarefied slip flow regime i.e., at an altitude of 80 km. We have carried out simulations using a compressible RANS based solver in the open source CFD software OpenFOAM [18]. To capture the rarefaction effects, we incorporate the first-order Maxwell slip boundary condition for velocity and Smoluchwoski boundary condition for temperature.

2 Numerical Simulations

OpenFOAM (Open Field Operation and Manipulation) is a popular open source CFD software which is parallel friendly and handles both the structured and unstructured meshes for complex geometries. It is based on C++ library tools and a collection of various applications (created using these libraries). Implementation of tensor fields, partial differential equations, boundary conditions and so on, can be handled using the libraries [19]. It has become a popular tool in the scientific and OpenSource community [20, 21].

2.1 *rhoCentralFoam*

The *rhoCentralFoam* is density-based compressible flow solver based on central upwind schemes of Kurganov and Tadmor [22, 23].

The *rhoCentralFoam* solver has been validated by Greenshields *et al.* [24] for supersonic jet experiment by Ladenburg *et al*. [25] and various standard compressible flow cases. Nakao *et al.* [26] have validated this solver against cryogenic wind tunnel data for sub-sonic flow around a NACA airfoil.

$k-\omega$ *SST* turbulence model is implemented in our simulations which is the mix of $k-\omega$ and $k-\varepsilon$ models. The *rhoCentralFoam* solver with $k-\omega$ *SST* turbulence model has been validated with analytical results for an electrospray RF ion Funnel [27] and with the experimental data for transonic turbulent flow over a deep cavity [28]. The $k-\omega$ model is used in the near-wall region, while $k-\varepsilon$ method is implemented in the fully turbulent region, i.e. away from the wall. The $k-\omega$ *SST* model is merited for its good behavior in adverse pressure gradients and separating flow [29, 30]. The shear stress transport (SST) formulation combines the best of two methods. Blending functions are implemented to assure a smooth transition between the $k-\omega$ model and the $k-\varepsilon$ model [31].

In current simulations, a calorically perfect ideal gas, air is used as the fluid for the nozzle flow. Transport properties are dependent on temperature and Sutherland viscos-

ity model has been used. One should note that no chemical reactions, ionization or dissociation phenomena are considered in current simulations.

2.2 Boundary conditions

The continuum regime of gas flows are simulated by using the conventional CFD techniques with the implementation of no-slip boundary condition for velocity and no-jump for temperature. However, for rarefied gas flows, experiments, and kinetic theory and particle simulation methods have shown that the no-slip/no-jump boundary conditions does not produce accurate flow predictions [32–34]. The degree of rarefaction is usually estimated based on the Knudsen number (Kn), which is the ratio of gas mean free path (λ) to the length scale of the system (L). It is also well established that the applicability of the CFD frame work can be extended upto the slip flow regime ($0.001 < Kn < 0.1$) with the application of non-equilibrium slip/jump boundary conditions [35].

The first order Maxwell velocity slip is defined as [36] :

$$U_f - U_w = \frac{2-\sigma_v}{\sigma_v}\lambda\frac{\partial u}{\partial y} + \frac{3}{4}\frac{\mu}{\rho T}\frac{\partial T}{\partial x}, \tag{1}$$

where U_f is the fluid velocity, U_w is the reference wall velocity, λ is the mean free path of gas, μ is dynamic viscocity, ρ is density of fluid, x is the axial co-ordinate, y is the normal co-ordinate, σ_v is tangential momentum accommodation coefficient and T is temperature.

Smoluchowski temperature jump is defined as [37,38] :

$$T_f - T_w = \frac{2-\sigma_T}{\sigma_T}\frac{2\gamma}{\gamma+1}\frac{\lambda}{Pr}\frac{\partial T}{\partial y}, \tag{2}$$

$$Pr = \frac{\mu c_p}{k}, \tag{3}$$

where T_f is the temperature of fluid, T_w is the reference wall temperature, Pr is the non-dimensional Prandtl number, σ_T is thermal accommodation coefficient, γ is specific heat ratio, c_p is specific heat and k is thermal conductivity.

Through out the current paper, we refer the results obtained using the *rhoCentralFoam* solver with the classical no-slip/no-jump boundary conditions as **no-slip**, while with the slip/jump boundary conditions (Eqs.1 and 2) is denoted as **slip**. Each test case is simulated in parallel on 32 Intel Haswell cores on the HPC facility at IIT Hyderabad.

3 Validations

3.1 Rothe Nozzle

The case that we have chosen to validate the *rhoCentralFoam* solver is Rothe nozzle [39]. Here, experiments are carried out to measure density and temperature data along the centre-line and radially at few critical locations. The computational domain consists of an axi-symmetric two degree wedge of the real nozzle. For this nozzle, an air flow is present at the inlet and a vacuum condition at the outlet. In this paper, the B = 590 case [39] of Rothe is chosen to be simulated, with an applied inlet pressure of 473.86 Pa and a temperature of 300 K [40]. The mesh of this test case is structured and consists of 24300 cells, where only one cell layer is placed in the symmetry direction. The side planes of the wedge are simulated as symmetry-planes by applying specular reflecting surfaces.

Here, the *rhoCentralFoam* solver is implemented with both the no-slip and slip boundary conditions and compared with experimental data [39] for temperature variations along the center-line of nozzle and along radial direction.

In the fig. 1a, the centerline profile of temperature is displayed. It can be seen that both the solvers produce reasonable results till an axial position of about 0.03 m after which slip CFD results are minutely deviated from the experimental data. This is because, molecular density being higher in the core region of nozzle flow, continuum effect is dominating along the centre-line and hence the no-slip values are more accurate. In the fig. 1b, the radial profile of the temperature is displayed. Here it can be seen that results of *rhoCentralFoam* solver with no slip boundary conditions are scattered from the experimental data. However, the *rhoCentralFoam* with slip boundary conditions manages to capture the validation temperature at the wall.

4 Test cases : Results and Discussion

The major objective of the current paper is to investigate the nozzle flow plume interaction with the surfaces of rocket model and back-flow effect for different divergence angles in the rarefied atmosphere. We chose the test case with Sonda II rocket model configuration [41] for external body, while the nozzle configuration is similar to Rothe [39] with a geometrical scale up of 4.75 times in all dimensions. Schematic of the test case is given in Figure 2.

Figure 3 demonstrates the computational domain used for simulations which is adaptively tested for normalized density gradients. The mesh is structured with multi-block grid and has 56000 cells.

Under-expanded plumes will expand freely and impinge back onto the walls of rocket adjacent to nozzle. Investigation is carried out on critical parts which are prone to back-flow and indeed where plume interaction takes place

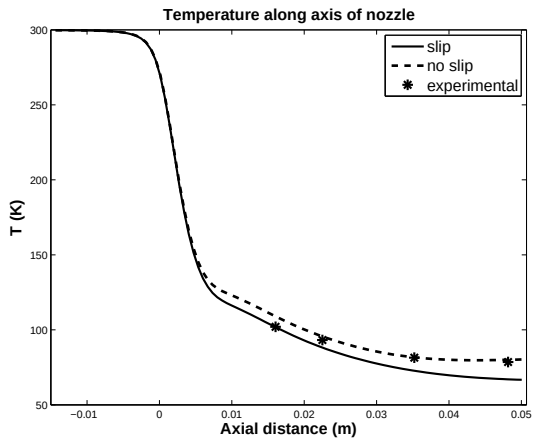

(a)

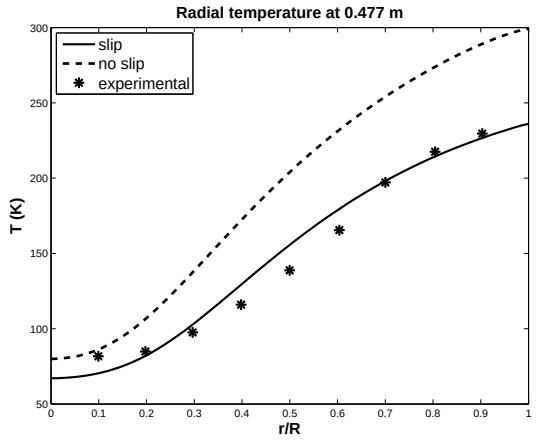

(b)

FIGURE 1: (a) Centre line temperature variation in the nozzle, where x = 0 denotes the throat location and (b) temperature variation in the radial direction at 0.0477m. Both slip and no slip solutions of *rhoCentralFoam* are compared with experimental data [39].

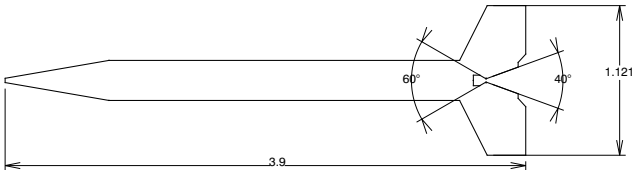

FIGURE 2: Schematic of Sonda II rocket [41] (dimensions in meters)

with a supersonic free-stream. Critical region under study is demonstrated in fig. 4 which is divided into two parts - critical zone 1 and critical zone 2. Critical zone 1 is where supersonic free-stream flow and plumes interact, while critical zone 2 is prone to backflow. Arc-length varies along the arrow from 0 to 0.748 for critical zone 1 and from 0.748 to 1.231 for critical zone 2.

We have carried out the parametric study for the two dimensional geometry of Sonda II model configuration (shown in figs. 2 and 3) in quiescent atmosphere at altitude of 80 km. Parameters include half-divergence angle variation of 12^0, 15^0 and 20^0. Steady state results are reported.

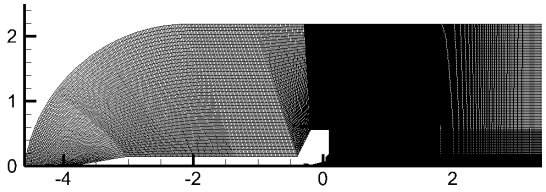

FIGURE 3: Computational domain of the test case with structured mesh.

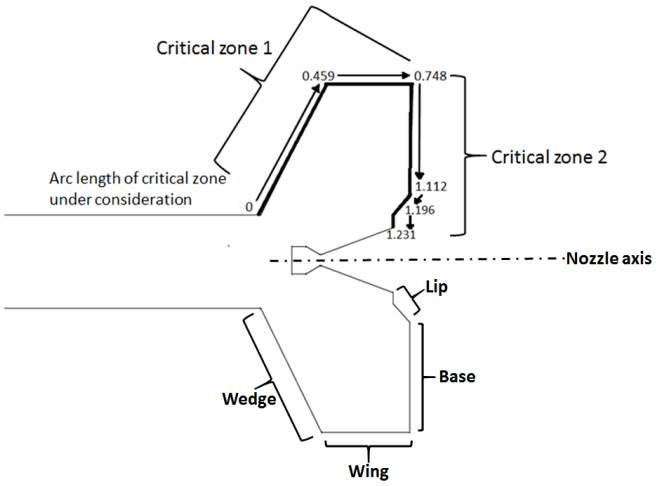

FIGURE 4: Zoomed view of Sonda II rocket schematic at the tail. The indicated bold line is the critical region of interest in the current study on which arc-length dimensions are denoted (dimensions in meters).

4.1 Coefficient of Pressure

The pressure coefficient C_p shows the dynamic relative pressure on the critical wall, which is defined as follows

$$C_p = \frac{p_w - p_\infty}{\frac{1}{2}\rho_\infty U_0^2}, \tag{4}$$

where p_w is the static pressure on the critical wall and ρ_∞ is the free-stream density. U_0 is calculated from chamber conditions. We define it as

$$U_0 = \sqrt{\gamma R T_0}, \tag{5}$$

where γ and R are specific heat ratio and gas constant for air respectively. And T_0 is the stagnation temperature in nozzle chamber which is 1000 K.

Figure 5 demonstrates the variation of pressure coefficient along the critical zone 1 (fig. 5a) and zone 2 (fig. 5b). C_p values in zone 1 are not much sensitive to change in divergent angle. Local minimum at the wedge-wing (arc-length $\sim$ 0.45 m) and wing-base corner (arc-length $\sim$ 0.74 m) is due to Prandtl Meyer expansion of plume back-flow. In critical zone 2, barrel shock is present at 1.15 m i.e. immediately after nozzle lip. Strength of barrel shock is very high for divergent angle 20^0 as compared to that of 15^0 and 12^0. This can be explained by the fact that the turning of the jet away from the nozzle axis is more influenced by divergence angle.

Table 1 demonstrates average C_p values on critical zones 1 and 2 for various divergence angles at 80 km altitude quiescent atmosphere conditions. Here, % deviation is defined as $\{(no\text{-}slip - slip)/\mid slip \mid \times 100\}$. It is observed that C_p values in critical zone 1 are not much sensitive to change in divergent angle, however, in critical zone 2, minimum C_p value is observed for divergent angle 15^0. % deviations are within 6.5 % and no-slip CFD predicts higher values than slip CFD.

TABLE 1: Average pressure coefficient values for different divergence angles at 80 km altitude in quiescent conditions in critical zone 1 and zone 2. Deviation is calculated in between slip and no-slip CFD for critical region 1 and 2.

Zone	Zone 1			Zone 2		
Divergent angle	12	15	20	12	15	20
Slip CFD	0.4151	0.4104	0.4217	4.8184	4.1534	6.3690
No-slip CFD	0.4143	0.4100	0.4216	5.0616	4.4177	6.7356
% Deviation	-0.2021	-0.0850	-0.0131	5.0486	6.3629	5.7559

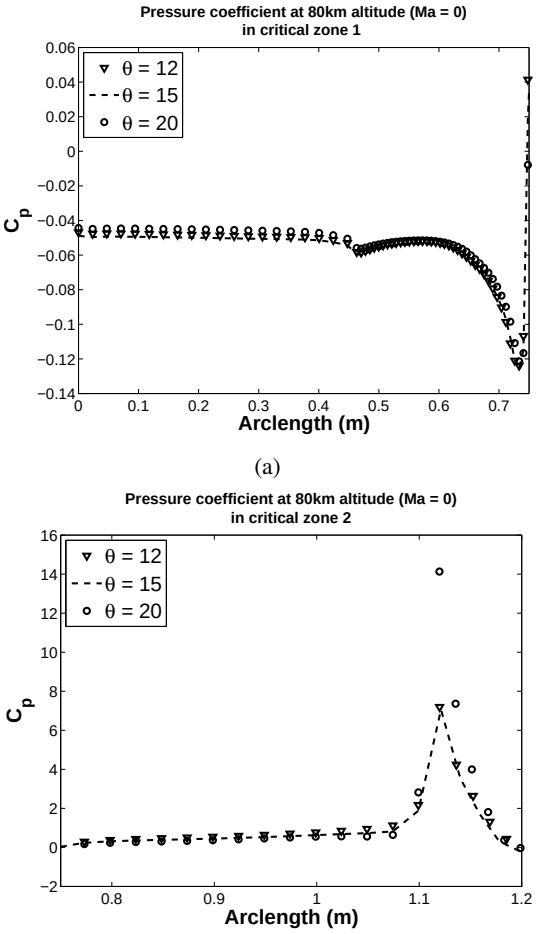

FIGURE 5: Variation of coefficient of pressure (C_p) along the arc length on critical zone 1 (fig a) & zone 2 (fig b) for different divergence angles at 80 km altitude conditions.

4.2 Coefficient of Drag

Coefficient of drag along a surface is a measure of net kinetic energy flux of the molecule impinging on the surface, which is defined by

$$C_D = \frac{\tau_w + p}{\frac{1}{2}\rho_\infty U_0^2}, \tag{6}$$

where τ_w is the wall shear stress on the critical region.

Drag force consists of 2 components, which are drag due to pressure difference and drag due to friction between fluid layer and solid wall.

Drag coefficient is negligible for all cases in critical zone 1 as there is no flow in that zone. Significant drag is present in the critical zone 2 because of direct impact of high

dense gas molecules on the wall. Similar to pressure coefficient, drag coefficient is observed to be minimum for 15^0 divergent angle. % deviations between slip and no-slip are within 7 %. Therefore, pressure and drag are not much sensitive to rarefaction and non-equillibrium effects.

TABLE 2: Average drag coefficient values for different divergence angles at 80 km altitude in quiescent conditions in critical zone 1 and zone 2. Deviation is calculated in between slip and no-slip CFD for critical region 1 and 2.

Zone	Zone 1			Zone 2		
Divergent angle	12	15	20	12	15	20
Slip CFD	0.2607	0.2568	0.2576	2.2441	2.1823	3.2566
No-slip CFD	0.2627	0.2588	0.2595	2.3394	2.3053	3.4753
% Deviation	0.7895	0.7852	0.7324	4.2504	5.6383	6.7138

4.3 Coefficient of Heat Transfer

Coefficient of heat transfer C_h along a surface is defined as follows,

$$C_h = \frac{q_w}{\frac{1}{2}\rho_\infty U_0^3}, \tag{7}$$

where q_w is the heat flux on the wall.

Figure 6 demonstrates the variation of heat transfer coefficient along the critical zone 1 (6a) and zone 2 (6b). In critical zone 1, C_h is found to be negative on the wedge shape (arc-length $\sim$ 0 - 0.45 m). Here, the ambient temperature (T_∞ = 196 K) being well below the fixed wall temperature (T_w = 300 K).

Table 3 demonstrates average C_h values on critical zones 1 and 2 for various divergence angles at 80 km altitude quiescent atmosphere conditions. Minimum of C_h is observed for 15^0 divergent angle nozzle. Significant % deviations are observed between slip and no-slip results as compared to C_p and C_D. In both the critical zones, no slip CFD results are over-predicting the slip results. The deviations are increasing with increase in divergence angle. This can be explained by the fact that exit velocity increases with increase in divergent angle and rapid expansion of plume jet leads to pressure below the ambient atmosphere. Therefore, more rarefaction on the critical region is observed which leads to major deviations. These findings may help the overall aero-thermodynamic design of a typical supersonic rocket model, which may lead to reduction in the weight of thermal protection systems along with lesser fuel usage.

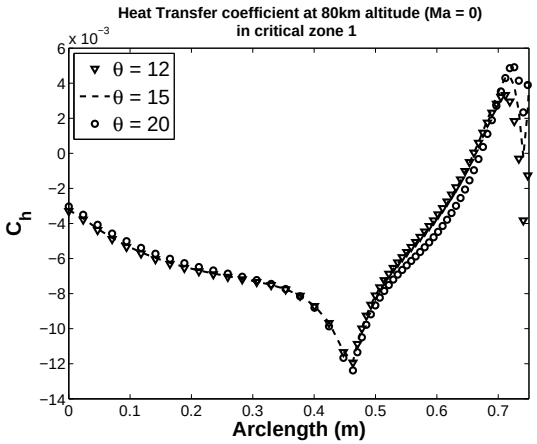

(a)

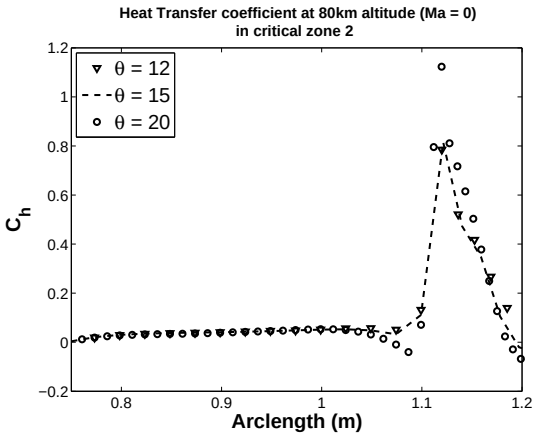

(b)

FIGURE 6: Variation of Heat transfer coefficient (C_h) along the arc length on critical zone 1 (fig a) & zone 2 (fig b) for different divergence angles at 80 km altitude conditions.

TABLE 3: Average heat transfer coefficient values for different divergence angles at 80 km altitude in quiescent conditions in critical zone 1 and zone 2. Deviation is calculated in between slip and no-slip CFD for critical region 1 and 2.

Zone	Zone 1			Zone 2		
Divergent angle	12	15	20	12	15	20
Slip CFD	-0.0045	-0.0043	-0.0045	0.1421	0.1245	0.1547
No-slip CFD	-0.0039	-0.0036	-0.0038	0.189	0.1841	0.2466
% Deviation	13.810	16.501	16.245	32.163	47.792	59.383

4.4 Coefficient of Trust coefficient

Thrust coefficient C_F of a nozzle is defined as follows,

TABLE 4: Trust coefficient values for different divergence angles at 80 km altitude in quiescent conditions

Divergent angle	12^0	15^0	20^0
C_f	2.1707	2.2320	2.3698

$$C_F = \frac{Thrust}{P_0 A_t}, \tag{8}$$

where P_0 is the chamber stagnation pressure and A_t is the throat area.

Thrust coefficient is dependent on exit pressure ratio, area ratio and specific heat ratio. Table 4 demonstrates calculated thrust coefficient values for different divergent angles and it is observed that value increases with increase in divergent angle.

5 CONCLUSION

We have presented aero-thermodynamic parameters on the critical region of rocket configuration where complex phenomenon of plume expansion and backflow occurs at high altitudes of 80 km conditions. Numerical simulations are carried out using the open source software OpenFOAM and implemented with both the no-slip and first order Maxwellian velocity slip and Smoluchwoski temperature jump boundary conditions. The latter boundary conditions consider non-equilibrium effects that exist due to very few collisions between the molecules in the flow around the rocket model which is due to rarefied conditions. The *rhoCentralFoam* solver is validated against experimental data for nozzle flow expanding in vacuum. We have carried out detailed investigations to report the non-equilibrium effects on the drag, pressure and heat transfer coefficients resulting because of plume impingement on the critical region of wall by comparing the conventional CFD results with the slip CFD results as well as their sensitivity towards nozzle divergence angle.

Nozzle with divergent angle 15^0 is found to be an optimum configuration, as it has moderate thrust coefficient and minimum drag and heat flux. It is observed that no-slip CFD predicts higher values of C_h than slip CFD which may lead to over-design of the critical zone in terms of thermal protection systems (TPS). It is evident the effect of rarefaction is more on heat transfer coefficient than pressure and drag coefficient. Hence, the accuracy of theoretical/continuum models for exhaust plumes back flow analysis in the slip and transition flow regimes cannot be decided based upon the mere comparisons for pressure coefficients alone, which are usually reported by experiments.

REFERENCES

[1] Glass, C., 1999. "A parametric study of jet interactions with rarefied flow". In International symposium on rarefied gas dynamics.

[2] Dettleff, G., and Grabe, M., 2011. Basics of plume impingement analysis for small chemical and cold gas thrusters. Tech. rep., DTIC Document.

[3] Love, E. S., and Grigsby, C. E., 1955. "Some studies of axisymmetric free jets exhausting from sonic and supersonic nozzles into still air and into supersonic streams".

[4] Adamson, T. C., and Nicholls, J. A., 1958. "On the structure of jets from highly underexpanded nozzles into still air: final report".

[5] Latvala, E., 1959. "Spreading of rocket exhaust jets at high altitudes". *ASTIA Document No. AD-215866, AEDC-TR-59-11 (June 1959).*

[6] Boynton, F. P., 1968. "Exhaust plumes from nozzles with wall boundary layers.". *Journal of Spacecraft and Rockets,* ***5***(10), pp. 1143–1147.

[7] Biju Kuttan, P., and Sajesh, M., 2013. "Optimization of divergent angle of a rocket engine nozzle using computational fluid dynamics". *Optimization,* ***2***(2), pp. 196–207.

[8] Patel, K. S., Reddy, K. S., Meshram, A. M., Chaphalkar, S., Khetre, S., Wankhede, S., El Hadim, B., El Minor, H., Adetoro, A., Adams, J., et al. "Flow analysis and optimization of supersonic rocket engine nozzle at various divergent angle using computational fluid dynamics (cfd)".

[9] Campbell, C., 1960. *Performance of several conical convergent-divergent rocket-type exhaust nozzles.*

[10] Krull, H. G., and Steffen, F. W., 1952. "Performance characteristics of one convergent and three convergent-divergent nozzles".

[11] Steffen, F. W., Krull, H. G., and Schmiedlin, R. F., 1954. *Effect of Divergence Angle on the Internal Performance Characteristics of Several Conical Convergent-divergent Nozzles.* National Advisory Committee for Aeronautics.

[12] Deissler, R., 1964. "An analysis of second-order slip flow and temperature-jump boundary conditions for rarefied gases". *International Journal of Heat and Mass Transfer,* ***7***(6), pp. 681–694.

[13] Zhang, W.-M., Meng, G., and Wei, X., 2012. "A review on slip models for gas microflows". *Microfluidics and nanofluidics,* ***13***(6), pp. 845–882.

[14] Guo, Z., Qin, J., and Zheng, C., 2014. "Generalized

second-order slip boundary condition for nonequilibrium gas flows". *Physical Review E,* ***89***(1), p. 013021.

[15] Lockerby, D. A., Reese, J. M., and Gallis, M. A., 2005. "Capturing the knudsen layer in continuum-fluid models of nonequilibrium gas flows". *AIAA journal,* ***43***(6), pp. 1391–1393.

[16] Dongari, N., Zhang, Y., and Reese, J. M., 2011. "Modeling of knudsen layer effects in micro/nanoscale gas flows". *Journal of Fluids Engineering,* ***133***(7), p. 071101.

[17] Lockerby, D. A., and Reese, J. M., 2008. "On the modelling of isothermal gas flows at the microscale". *Journal of Fluid Mechanics,* ***604***, pp. 235–261.

[18] Fundation, O., 2014. "Openfoam". *The Open Source CFD Toolbox. User Guide. Open-FOAM Fundation*.

[19] Weller, H. G., Tabor, G., Jasak, H., and Fureby, C., 1998. "A tensorial approach to computational continuum mechanics using object-oriented techniques". *Computers in physics,* ***12***(6), pp. 620–631.

[20] Jasak, H., 2010. "Openfoam: a year in review". In 5th OPENFOAM Workshop, Gothenburg, Sweden, June, pp. 21–24.

[21] Casartelli, E., and Mangani, L., 2013. "Object-oriented open-source cfd for turbomachinery applications: A review and recent advances". In ASME Turbo Expo 2013: Turbine Technical Conference and Exposition, American Society of Mechanical Engineers, pp. V06BT37A036–V06BT37A036.

[22] Kurganov, A., and Tadmor, E., 2000. "New high-resolution central schemes for nonlinear conservation laws and convection–diffusion equations". *Journal of Computational Physics,* ***160***(1), pp. 241–282.

[23] Kurganov, A., Noelle, S., and Petrova, G., 2001. "Semidiscrete central-upwind schemes for hyperbolic conservation laws and hamilton–jacobi equations". *SIAM Journal on Scientific Computing,* ***23***(3), pp. 707–740.

[24] Greenshields, C. J., Weller, H. G., Gasparini, L., and Reese, J. M., 2010. "Implementation of semi-discrete, non-staggered central schemes in a colocated, polyhedral, finite volume framework, for high-speed viscous flows". *International journal for numerical methods in fluids,* ***63***(1), pp. 1–21.

[25] Ladenburg, R., Van Voorhis, C., and Winckler, J., 1949. "Interferometric studies of faster than sound phenomena. part ii. analysis of supersonic air jets". *Physical Review,* ***76***(5), p. 662.

[26] Nakao, S., Kashitani, M., Miyaguni, T., and Yamaguchi, Y., 2014. "A study on high subsonic airfoil flows in relatively high reynolds number by using openfoam". *Journal of Thermal Science,* ***23***(2), pp. 133–137.

[27] Tridas, E. M., 2012. "Experimental and numerical investigation of an electrospray rf ion funnel".

[28] Freitas, P., 2014. "Numerical simulation of compressible flow over a deep cavity".

[29] Menter, F. R., 1993. "Zonal two equation k-turbulence models for aerodynamic flows". *AIAA paper,* ***2906***, p. 1993.

[30] Menter, F., Kuntz, M., and Langtry, R., 2003. "Ten years of industrial experience with the sst turbulence model". *Turbulence, heat and mass transfer,* ***4***(1).

[31] Davidson, L., 2011. "Fluid mechanics, turbulent flow and turbulence modeling". *Chalmers University of Technology, Goteborg, Sweden (Nov 2011)*.

[32] Arkilic, E. B., Schmidt, M. A., and Breuer, K. S., 1997. "Gaseous slip flow in long microchannels". *Microelectromechanical Systems, Journal of,* ***6***(2), pp. 167–178.

[33] Colin, S., 2005. "Rarefaction and compressibility effects on steady and transient gas flows in microchannels". *Microfluidics and Nanofluidics,* ***1***(3), pp. 268–279.

[34] Gad-el Hak, M., 1999. "The fluid mechanics of microdevicesthe freeman scholar lecture". *Journal of Fluids Engineering,* ***121***(1), pp. 5–33.

[35] Bird, G., 1994. "Molecular gas dynamics and the direct simulation monte carlo of gas flows". *Clarendon, Oxford,* ***508***.

[36] Maxwell, J. C., 1867. "On the dynamical theory of gases". *Philosophical transactions of the Royal Society of London*, pp. 49–88.

[37] Le, N. T., White, C., Reese, J. M., and Myong, R. S., 2012. "Langmuir–maxwell and langmuir–smoluchowski boundary conditions for thermal gas flow simulations in hypersonic aerodynamics". *International Journal of Heat and Mass Transfer,* ***55***(19), pp. 5032–5043.

[38] Mahdavi, A.-M., Le, N. T., Roohi, E., and White, C., 2014. "Thermal rarefied gas flow investigations through micro-/nano-backward-facing step: Comparison of dsmc and cfd subject to hybrid slip and jump boundary conditions". *Numerical Heat Transfer, Part A: Applications,* ***66***(7), pp. 733–755.

[39] Rothe, D. E., 1971. "Electron-beam studies of viscous flow in supersonic nozzles". *AIAA Journal,* ***9***(5), pp. 804–811.

[40] Ivanov, M., Markelov, G., Ketsdever, A., and Wadsworth, D., 1999. *Numerical study of cold gas micronozzle flows*. American Institute of Aeronautics and Astronautics.

[41] Bigarella, E., Azevedo, J. L. F., and Mello, O., 2004. "Normal force calculations for rocket-like configurations". *Journal of the Brazilian Society of Mechanical Sciences and Engineering,* ***26***(3), pp. 290–296.